Interventional Dual-Energy Imaging - Feasibility of rapid kV-switching on a C-Arm CT System

K. Müller,[1] S. Datta,[2,*] M. Ahmad,[1] J.-H. Choi,[1] T. Moore,[2]
L. Pung,[2] C. Niebler,[3] G. E. Gold,[4,5,6] A. Maier,[7,†] and R. Fahrig[1,‡]

[1]*Radiological Sciences Lab, Stanford University, Stanford, CA, USA*
[2]*Siemens Medical Solutions Inc., Malvern, PA*
[3]*Department of Electrical Engineering, Technische Hochschule Nürnberg, Germany*
[4]*Department of Radiology, Stanford University, Stanford, CA, USA*
[5]*Department of Orthopaedic Surgery, Stanford University, Stanford, CA, USA*
[6]*Department of Bioengineering, Stanford University, Stanford, CA, USA*
[7]*Pattern Recognition Lab, Friedrich-Alexander-Universität Erlangen-Nürnberg, Erlangen, Germany*

(Dated: September 27, 2016)

Abstract

Purpose: In the last years, dual-energy CT imaging has shown clinical value thanks to its ability to differentiate materials based on their atomic number and to exploit different properties of images acquired at two different energies. C-arm CT systems are used to guide procedures in the interventional suite. Up to now, there are no commercially available systems that employ dual-energy material decomposition. This paper explores the feasibility of implementing a fast kV-switching technique on a clinical available angiographic system for acquiring dual-energy C-arm CT images.

Methods: As an initial proof of concept, a fast kV-switching approach was implemented on an angiographic C-arm system and the peak tube voltage during 3D rotational scans was measured. The tube voltage measurements during fast kV-switching scans were compared to corresponding measurements on kV-constant scans. Additionally, to prove stability of the requested exposure parameters, the accuracy of the delivered tube current and pulse width were also recorded and compared. In a first phantom experiment, the voxel intensity values of the individual tube voltage components of the fast kV-switching scans were compared to their corresponding kV-constant scans. The same phantom was used for a simple material decomposition between different iodine concentrations and pure water using a fast kV-switching protocol of 81 and 125 kV. In the last experiment, the same kV-switching protocol as in the phantom scan was used in an *in vivo* pig study to demonstrate clinical feasibility.

Results: During rapid kV-switching acquisitions, the measured tube voltage of the X-ray tube during fast switching scans has an absolute deviation of 0.23 ± 0.13 kV compared to the measured tube voltage produced during kV-constant acquisitions. The stability of the peak tube voltage over different scan requests was about 0.10 kV for the low and 0.46 for the high energy kV-switching scans and less than 0.1 kV for kV-constant scans, indicating slightly lower stability for kV-switching scans. The tube current resulted in a relative deviation of -1.6% for the low and 6.6% overestimation for the high tube voltage of the kV-switching scans compared to the kV-constant scans. The pulse width showed no deviation for the longer pulse width and only minor deviations (0.02 ± 0.02 ms) for the shorter pulse widths compared to the kV-constant scans. The phantom experiment using different iodine concentrations showed an accurate correlation ($R^2 > 0.99$) between the extracted intensity values in the kV-switching and kV-constant reconstructed volumes, and allows for an automatic differentiation between contrast concentration down to 10% (350 mg/mL iodine) and pure water under low-noise conditions. Preliminary results of iodine and soft tissue separation

showed also promising results in the first *in vivo* pig study.

Conclusion: The feasibility of dual-energy imaging using a fast kV-switching method on an angiographic C-arm CT system was investigated. Direct measurements of beam quality in the X-ray field demonstrate the stability of the kV-switching method. Phantom and *in vivo* experiments showed that images did not deviate from those of corresponding kV-constant scans. All performed experiments confirmed the capability of performing fast kV-switching scans on a clinical available C-arm CT system. More complex material decomposition tasks and post-processing steps will be part of future investigations.

* Now with Case Western Reserve University School of Medicine, Cleveland, OH, USA

† Also with the Erlangen Graduate School in Advanced Optical Technologies (SAOT), Erlangen, Germany

‡ Now with Siemens Healthcare GmbH, Forchheim, Germany

I. INTRODUCTION

C-arm angiography is the primary imaging modality used during minimally invasive procedures for navigation of interventional devices. These C-arm angiographic systems are capable of guiding the physician using fluoroscopic 2D X-rays at frame rates up to 30 f/s. Furthermore, they allow acquisition of 2D X-ray images during rotational scans. These X-ray images acquired under different projection angles can be used for a 3D reconstruction of the field-of-view using a cone-beam reconstruction (FDK) algorithm [1]. The 3D reconstructions are clinically used for numerous applications, including liver cancer treatment in interventional oncology [2], providing additional navigational support during transcatheter structural heart interventions [3] or cerebral aneurysms assessment in neuroradiology [4].

In the last decade, dual-energy imaging in conventional CT has grown in clinical use [5–9]. This technique allows the differentiation of materials and tissue based on differential absorption of varying X-ray photon energies [10]. For example, iodine, a commonly used vascular contrast agent, shows sharply decreasing attenuation with increasing X-ray energy due to the photo-electric effect. This spectral response is different than that of soft tissue which shows more constant attenuation due mostly to Compton scattering. Acquiring X-ray projection images at different photon energies requires two consecutive scans with two different tube potentials (consecutive technique), a multilayer detector (multilayer technique), a photon-counting energy-discrimination detector (photon counting technique), two simultaneously operating X-ray tubes (dual-source technique), or one X-ray tube with rapid modulation of the tube voltage (fast kV-switching technique) [11].

Within interventional radiology, dual-energy imaging is still ongoing research, including development of photon counting detectors with dual-energy capabilities [12–15]. Interventional dual-energy imaging would allow, for example, differentiation of iodinated contrast agent and haemorrhage directly after revascularisation in acute ischaemic stroke patients [16]. Also 3D spectral imaging during the intervention may permit depiction of the vascular lumen while separating it from calcified plaque and/or different contrast agent [17]. Detailed material differentiation within the interventional suite directly during or after the treatment would allow adjustment of respective therapy planning immediately.

In this paper, the hypothesis that fast kV-switching dual-energy imaging is possible with an interventional angiography system using only one sweep of the C-arm is investigated. The

system is equipped with one X-ray tube and can be used to generate images at different X-ray energies by switching the X-ray tube voltage rapidly from pulse to pulse. To date, there is no clinically available angiographic C-arm system available allowing dual-energy imaging during a single rotational 3D acquisition. In a first experiment, tube voltage measurements were performed to prove the concept of kV-switching with the C-arm system and to measure any instability resulting from rapidly switching the tube voltage. A fast kV-switching protocol was used to image an electron density phantom with different iodine concentrations, and a first *in vivo* study was carried out. Preliminary results on the feasibility have been presented in Datta et al. [18], where one specific rapid kV-switching set up has been evaluated with respect to only one iodine concentration (500 mg I; 10 mg/mL) within a water-like phantom. This first limited study encouraged us to investigate multiple rapid kV-switching setups in a phantom and in an *in vivo* study.

II. METHODS AND MATERIALS

A. C-arm CT: kV-Switching Principle

In general, an automatic exposure control (AEC) software is integrated in C-arm systems in order to maintain the same detector entrance dose throughout the scan while rotating around the patient [19]. The software adapts the tube current (mA), pulse width (ms), and tube voltage (kV) in order to maintain a constant detector entrance dose. That means the exposure varies dynamically based on the projection angle and attenuation of the object in the field of view. In order to perform dual-energy C-arm CT imaging, constant tube voltage settings are required. In this study, a prototype software application enables manual control of the tube output on a research Artis zeego C-arm angiography system (Siemens Healthcare GmbH, Forchheim, Germany). The prototype uses a modifiable configuration file that allows acquisition of projection images with pre-defined acquisition parameters: kVp, mA, and ms for each X-ray pulse. Each 3D acquisition resulted in 248 projections over an angular range of 200 degrees over a time duration of 10 s with an angular increment of 0.8° between adjacent 2D X-ray images. No copper filtration is used in addition to the system's fixed filtration of 2.5 mm aluminum. The acquired 2D projection images have an isotropic pixel size of 0.616 mm. For the kV-switching scan, there were 124 projections acquired at a low

tube voltage interleaved with 124 projections acquired at a high tube voltage. The current and pulse width parameters for the scans were chosen to match the current and pulse width parameters the system reports during a clinical scan of a body phantom with the AEC on, with a dose request of $1.2\mu Gy/f$ and the respective tube voltage. The sets of projections were separated and reconstructed individually for the low and high energy datasets with a filtered-backprojection algorithm. To facilitate a head-to-head comparison, kV-constant acquisitions were undersampled by removing alternating projections before reconstruction. The 2D X-ray projection images were pre-processed according to the actual exposure parameters used. All volumes were reconstructed with an isotropic voxel size of 1 mm distributed on a 256^3 grid size. No additional post-processing algorithms were applied.

B. Calibration of kV Meter using Fixed Exposure Parameter

In order to assess the C-arm system's capability of switching high and low tube voltage between adjacent frames during a 3D rotational scan, a kV meter was used to measure the respective peak tube voltage within the X-ray beam spectrum. First, to assess the consistency of the kV meter to measure the system tube voltage for 2D and 3D imaging, the tube voltage was measured using sequences with fixed exposure parameter settings.

For both experiments, the tube voltage was measured within the X-ray beam path using a non-invasive kV meter from *Radcal® Accu-Gold with an AGMS-D* sensor. The sensor has a range from 40-160 kV and a nominal accuracy of ±2.5%. The calibration of this device can be traced to the Accredited Dosimetry Calibration Laboratory (ADCL) calibration. In measuring the peak voltage of the X-ray beam, the general recommendations of AAPM Report #74 (Quality Control in Diagnostic Radiology) were followed [20]. Although kV meters are typically suspended in air during measurements, the kV meter was attached to the face of the flat panel detector in order to maintain the appropriate source/kV-meter orientation during a C-arm rotation. It was verified that any backscatter contribution to the kV meter reading was negligible ($< 1\%$). From the datasheet of the installed X-ray generator an accuracy of the X-ray tube (MEGALIX CAT Plus) of ±5% can be assumed.

C. 3D Tube Voltage Measurement using fast kV-Switching

For evaluation of the stability of the kV-switching scans, the tube current was held constant at 100, 200, or 300 mA and four different fast kV-switching settings were investigated. The tested kV-switching protocols had low and high kVp of 70/90, 70/109, 81/109, and 81/125 kV with 100, 200, and 300 mA, and with 12.5 ms and 3.2 ms pulse width for the low and the high energies. It is noted that a fast kV-switching scan between 70 kV and 125 kV is not possible when a similar detector entrance dose is preferred for both low and high energies. Rapidly switching the current between low and high tube voltage settings is not possible because that is controlled by changing the temperature of the filament. The system's minimal pulse width is 3.2 ms and the maximum pulse width is 12.5 ms. Therefore, a fast kV-switching scan between 70 and 125 kV would result in underexposed 70 kV images or overexposed 125 kV images.

D. Contrast Concentration Measurements

The next experiment was an iodine contrast concentration benchmark evaluation using the same 3D scan protocol as described in Section II A. The inner disk of the electron density phantom (model M062) from *CIRS* was loaded with eight 20 mL syringes. The syringes were filled with iodinated contrast (Omnipaque 350 mg/mL) with different concentrations (0%, 5%, 10%, 12.5%, 25%, 50%, 75%, and 100%), as well as a dense bone sample (1.82 g/cc physical density). Taking into consideration the possible kV-switching range of the previous experiment in Section II C, four different kV-switching combinations were performed: 70/90 kV (12.5/3.3 ms, 350 mA), 81/109 kV (12.5/3.3 ms, 225 mA), 90/125 kV (12.5/3.2 ms, 250 mA), and 81/125 kV (12.5/3.2 ms, 225 mA). Tube current was selected such that no severe under or overexposure of the phantom will appear in the acquired X-ray low and high energy projection images.

E. In vivo Experiment

The capability of the kV-switching method of dual-energy imaging was also tested *in vivo*. The protocol for this *in vivo* animal study was approved by Stanford University's Administrative Panel on Laboratory Animal Care. One Yorkshire pig (approximately 50

kg) was used for this study. Arterial femoral access was established using percutaneous puncture for hemodynamic monitoring, administration of medications, and the injection of contrast agent. First, two constant scans with 81 kV, 295 mA, and 12.5 ms and 125 kV, 295 mA, and 3.2 ms were performed, followed by the fast kV-switching scan using the same parameters. Again, tube current was selected such that no severe under or overexposure of the pig will appear in the 2D acquired projection X-ray images. All scans were performed during administration of a 17 mL bolus of 50% iodinated contrast agent (Omnipaque 350 mg/mL) diluted in saline. The contrast was administered with a rate of 1.5 mL/s through a 5F Envoy guiding catheter (Codman, Raynham, MA) positioned proximally within the external carotid artery using a power injector (Medtron, Saarbrücken, Germany). An X-ray imaging delay of 1s was used.

For the *in vivo* data, from the high and low energy 3D reconstructions, a dual-energy index (DEI) volume is computed according to Johnson et al. [21]:

$$\mathrm{DEI} = \frac{HU_{81kV} - HU_{125kV}}{HU_{81kV} + HU_{125kV} + 2000}. \tag{1}$$

The DEI is zero for water, negative for atoms with a smaller and positive for atoms with a larger effective atomic number Z than water.

III. RESULTS AND DISCUSSION

A. Calibration of kV Meter using Fixed Exposure Parameter

The tube voltage was measured for different fixed combinations of exposure parameters described in Section II B for 2D imaging and a frame rate of 10 fps. Table I summarizes the requested and the resulting measured tube voltage, and the percentage error. Figure 1, shows the correlation ($R^2 > 0.99$) between the requested and the measured tube voltage. Overall, the measurements result in an absolute error of 1.47 ± 0.73 kV and a relative $1.45 \pm 0.54\%$ overestimation of the requested tube voltage, which lies within the output uncertainty of the X-ray source and the measurement accuracy of the kV meter. The 2D tube voltage measurements were stable for multiple acquisitions, various requested currents, and different pulse widths. For 3D rotational acquisitions, various exposure parameters were requested in order to characterize the tube voltage stability. Here, a typical frame rate of 30 fps was chosen. Table II shows the requested tube voltage, the measured tube voltage,

Requested tube voltage [kV]	Estimated tube voltage [kV]	Error [%]
70	70.30	0.43
81	82.15	1.42
90	91.50	1.64
109	110.95	1.79
125	127.45	1.96
		1.45 ± 0.54

Table I. 2D tube voltage requests, their respective tube voltage estimations, and the percentage error.

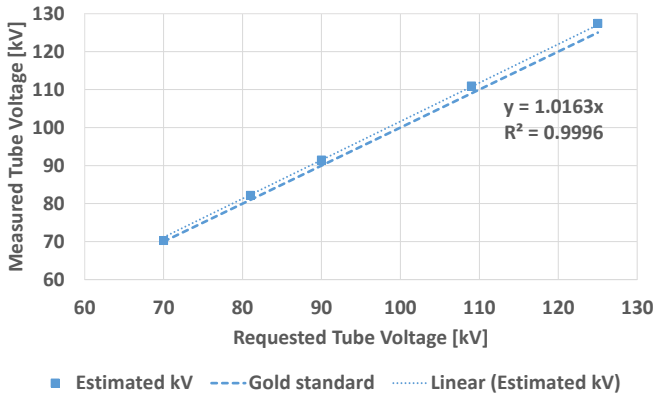

Figure 1. Correlation between requested and measured tube voltage measurements during 2D acquisitions ($R^2 > 0.99$).

Requested tube voltage [kV]	Estimated tube voltage [kV]	Error [%]
50	49.57 ± 0.54	0.87
70	69.97 ± 0.35	0.36
81	81.52 ± 0.58	0.75
90	88.52 ± 2.25	1.88
109	105.77 ± 3.06	2.97
125	119.91 ± 4.13	4.07
		1.82 ± 1.33

Table II. 3D tube voltage request, the respective tube voltage estimations, and the percentage error.

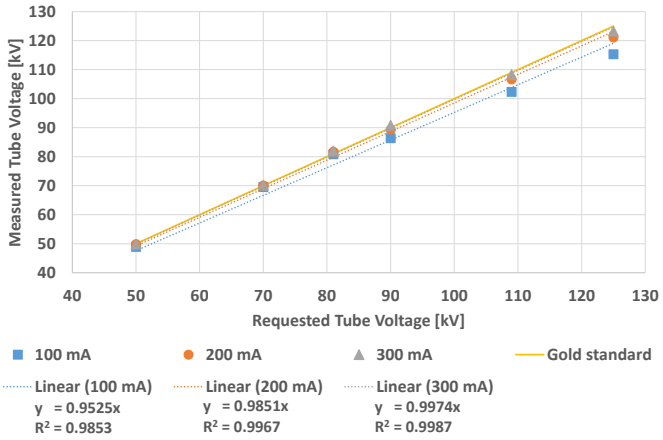

Figure 2. Correlation between requested and measured tube voltage measurements during 3D acquisitions.

and the respective computed percentage error. All results were averaged over different currents (100 mA, 200 mA, and 300 mA). The minimum error was higher than for the 3D scans compared to the 2D acquisitions with a percentage deviation of $1.82 \pm 1.33\%$. Figure 2 shows the correlation between the requested and measured tube voltage for the different current. The plot shows a slightly higher deviation in the delivered tube voltage as requested tube voltage increases for small tube current (100 mA).

B. 3D Tube Voltage Estimation using fast kV-Switching

The experiments in Section III A show that the deviation of the measured and requested tube voltage is within the nominal accuracy of the kV meter. For the fast kV-switching acquisitions the four different settings described in Section II C have been used. In Figure 3, the deviation in tube voltage [kV], current [mA] and pulse width [ms] between the different fast kV-switching and their respective constant is shown. Overall the measured kVp in the lower tube voltage pulse deviates from the constant scan measurement by 0.29 ± 0.10 kV and in the higher tube voltage pulse by 0.16 ± 0.12 kV (c.f. Figure 3a). Figure 3b also shows that the absolute error in kV is less than 0.5 kV for the fast kV-switching scans compared to their respective constant scans. Figure 3c shows the difference for the current between the constant and the kV-switching scans. During constant scans at high energy, a reduced current is delivered compared to the requested current, especially when the requested current increases. This is in order to reduce the overall tube load over a 3D scan. Consequently, the deviation in current (Figure 3d) is larger between the constant and fast kV-switching scans, while the kV-switching scan delivers a more accurate current. The accuracy of the pulse width is given in Figure 3e. For the longer pulse width no deviation in the stability of the pulse width was measured, the short pulse width resulted in 0.02 ± 0.02 ms deviation to the requested pulse width (Figure 3f). The variation of the measured peak tube voltage among X-ray pulses was about 0.10 kV for the low and 0.46 for the high energy request during kV-switching scans and less than 0.1 kV for kV-constant scans, indicating slightly lower stability for kV-switching scans. Overall it can be observed that the accuracy of the delivered tube voltage deviates only slightly between constant and fast kV-switching scans. The delivered current mismatch slightly increases with higher requested current at higher tube voltage, also measurable in the deviation of the delivered pulse width.

C. Contrast Concentration Measurements

For the iodine contrast concentration benchmark evaluation as described in Section II D, the HU values in the electron density phantom between the fast kV-switching and their respective undersampled constant scan were correlated. Therefore, in every syringe a region of interest (ROI) was placed and the mean HU value was extracted (c.f. Figure 4). An

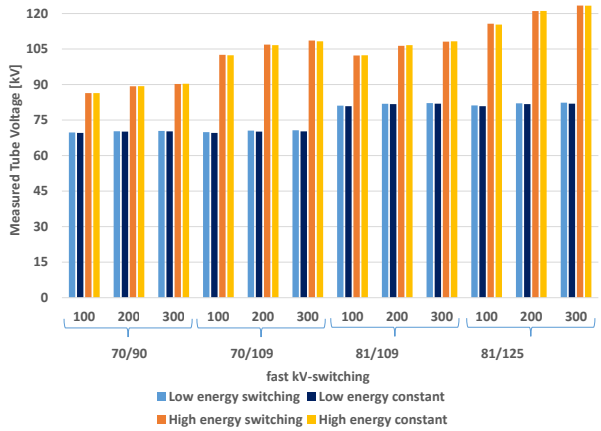

(a)

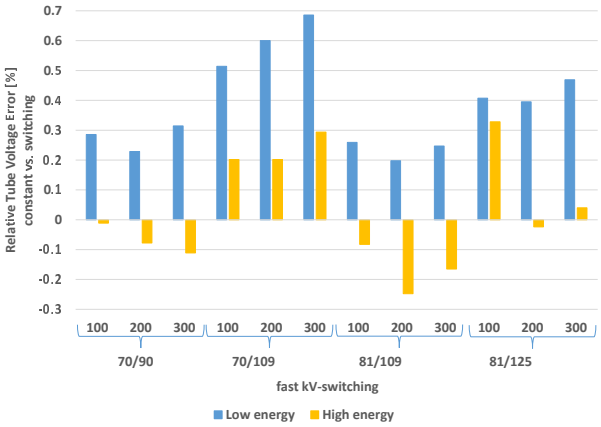

(b)

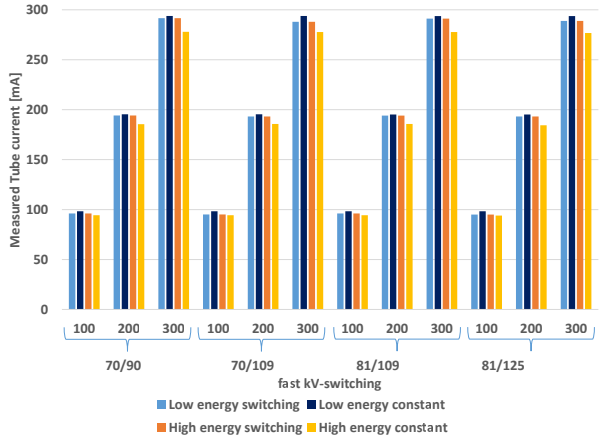

(c)

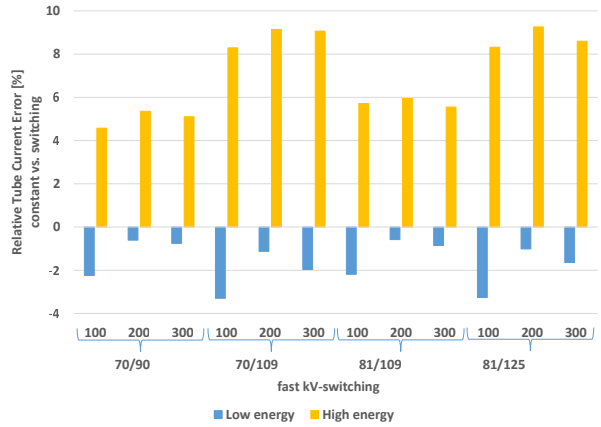

(d)

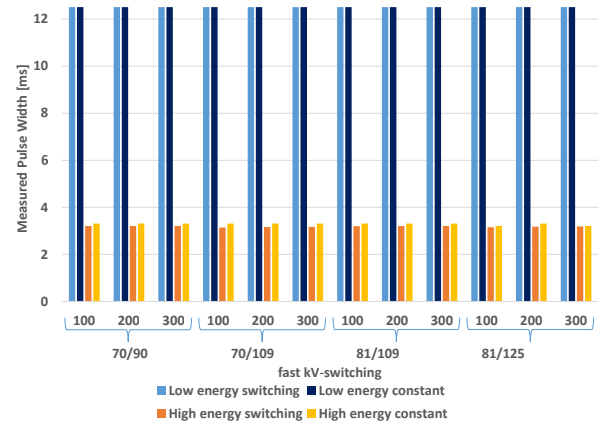

(e)

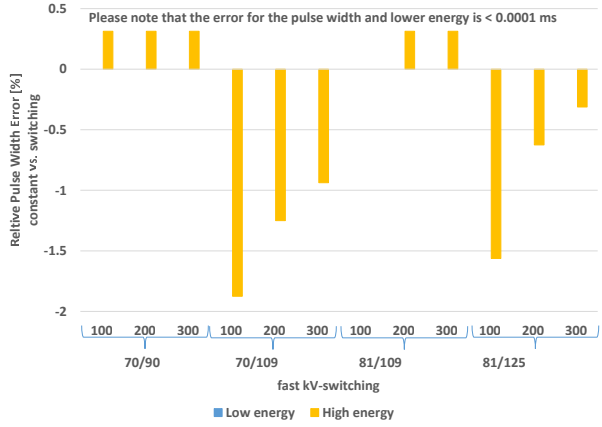

(f)

Figure 3. Requested and measured (a) tube voltage [kV], (c) tube current [mA], and (e) pulse width [ms] during different fast kV-switching combinations. Absolute error of (b) tube voltage [kV], (d) tube current [mA], and (f) pulse width [ms] between kV-switching and their respective constant scans.

excellent correlation ($R^2 > 0.99$) between the undersampled constant extracted ROIs and their respective fast kV-switching ROIs was achieved over the various scan parameters (Figure 5). Figure 6 shows the potential for the 81 kV and 125 kV switching scan to visually differentiate various contrast concentrations from pure water. Axial slices from the 3D reconstructions from the various kV-switching settings and a noise measurement taken as the standard deviation in HU (σ_w) within the pure water syringe can be found in Figure 7. The axial slice from the respective 3D reconstructions from the 81 kV and 125 kV switching scan are shown in Figure 7j and 7k. The difference image in Figure 7l confirms the differentiation of the water-like background from the iodine samples down to 10% and the bone insert. However, the iodine sample of 5% is hardly visible in the difference image due to the low concentration in the syringe and because of interfering artifacts from undersampling and the photon starvation in the high concentration syringe. A clinical contrast concentration ranges from 100% down to 25%. Therefore, the tested contrast agent detectability by dual-energy imaging is sensitive to clinical iodine concentrations.

D. In vivo Experiment

For the *in vivo* animal scan, the HU values between the fast kV-switching and the respective undersampled constant scan were correlated. An ROI was placed in a homogenous soft tissue region, bone marrow, dense bone, and within a contrasted vessel (Figure 8). For each ROI the mean HU value was extracted. The correlation between undersampled constant and fast kV-switching HU values resulted in $R^2 > 0.99$ (Figure 9). An increase in contrast for 81 kV between iodine and water can be seen compared to the 125 kV reconstruction. Figure 10a and 10b show an axial slice of the low and high energy 3D reconstruction from the fast kV-switching scan. The 81 kV data shows more prominent noise, but better contrast visibility compared to the 125 kV that exhibits less noise, but also less contrast within the soft tissue. In Figure 10c, the corresponding DEI map after applying a 3D median filter to reduce noise and streak artifacts is shown. The contrast agent (50% diluted), can be visually separated from bone and soft tissue by using a color coding map. Figure 10d, 10e, and 10f show the respective undersampled constant scan results.

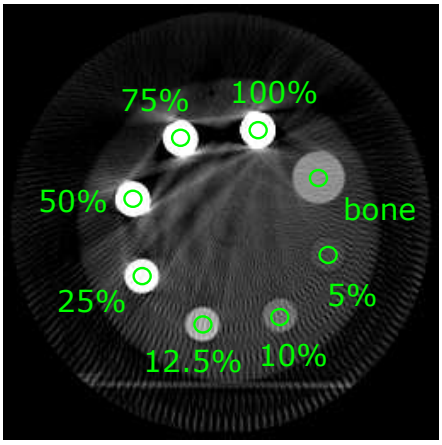

Figure 4. Axial slice of 3D reconstruction of switching scan of 81 kV with measured ROIs in different syringes filled with different iodine concentrations and a bone dense material (C 2300 HU, W 6300 HU).

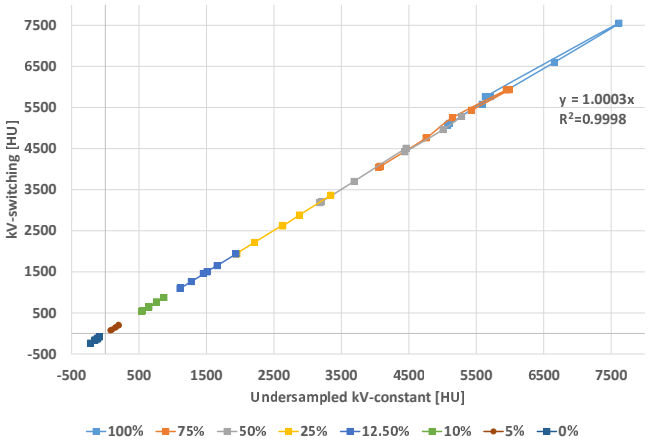

Figure 5. Correlation of HU values measured in the different syringes in the kV-switching and in the respective 50% undersampled constant scans ($R^2 > 0.99$).

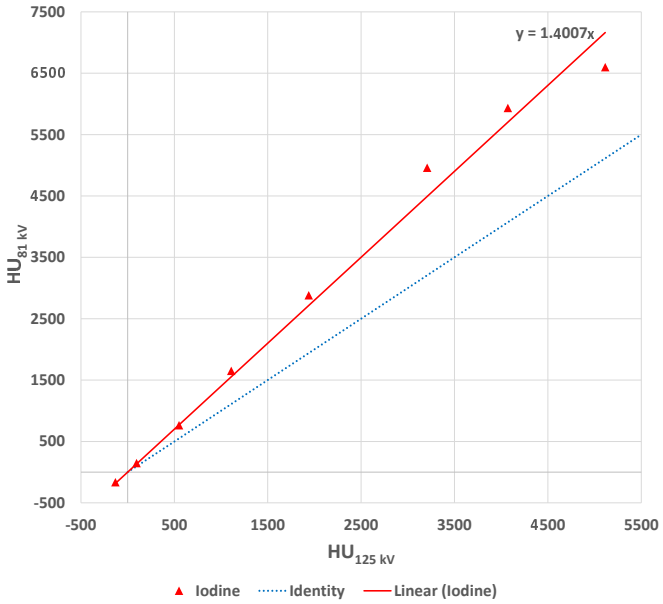

Figure 6. Measurable change in iodine HU values as function of kV for the fast kV-switching scan of 81 kV and 125 kV.

IV. CHALLENGES AND LIMITATIONS

Fast kV-switching protocols that were possible with the angiographic system were switching between 81 kV and 125 kV which is the maximum possible tube voltage difference. The maximum tube voltage that can be achieved with this X-ray tube is 125 kV, which is lower

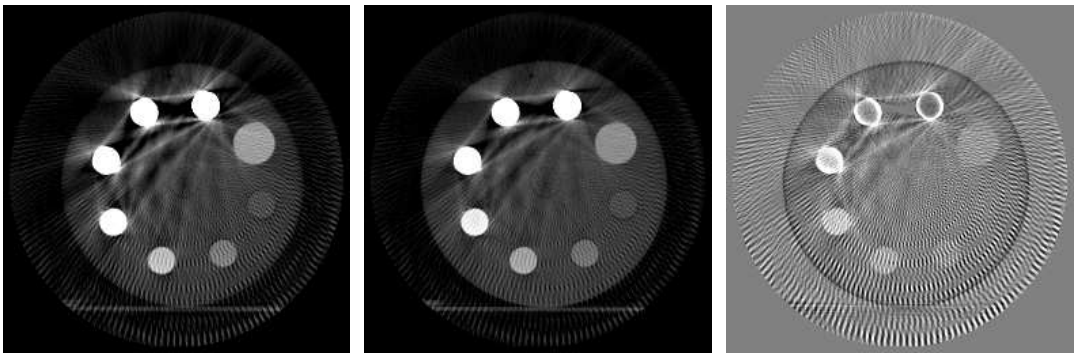

(a) 70 kV; $\sigma_w = 89.42$ HU (b) 90 kV; $\sigma_w = 63.48$ HU (c) Difference (a)-(b)

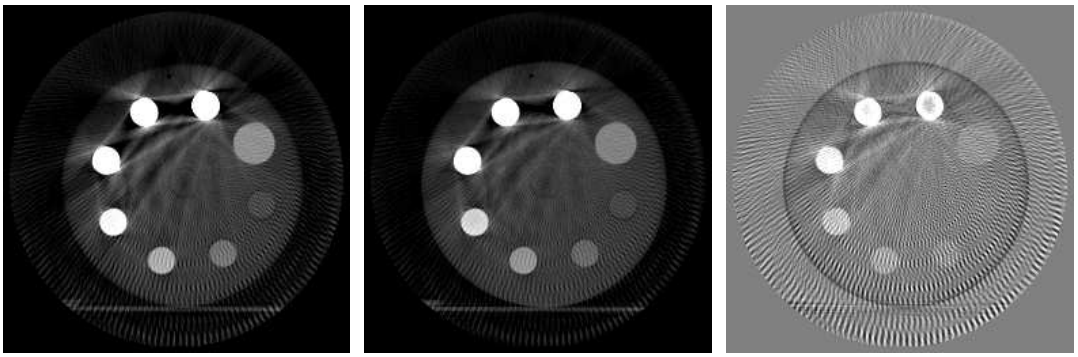

(d) 81 kV; $\sigma_w = 63.34$ HU (e) 109 kV; $\sigma_w = 46.11$ HU (f) Difference (d)-(e)

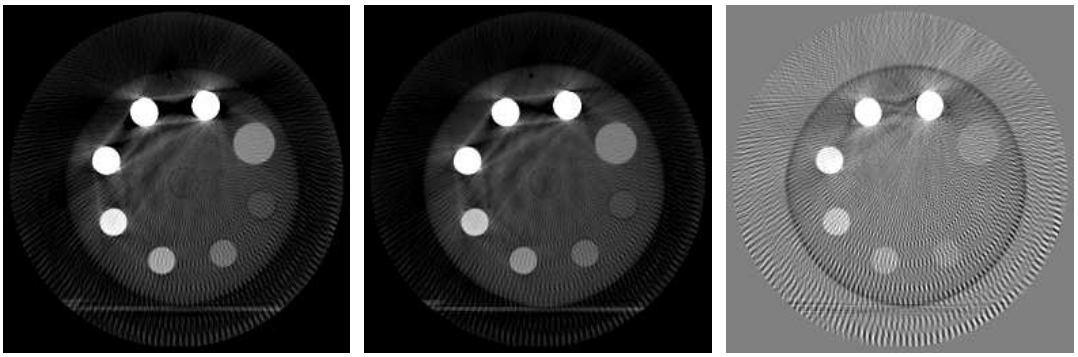

(g) 90 kV; $\sigma_w = 45.07$ HU (h) 125 kV; $\sigma_w = 43.19$ HU (i) Difference (g)-(h)

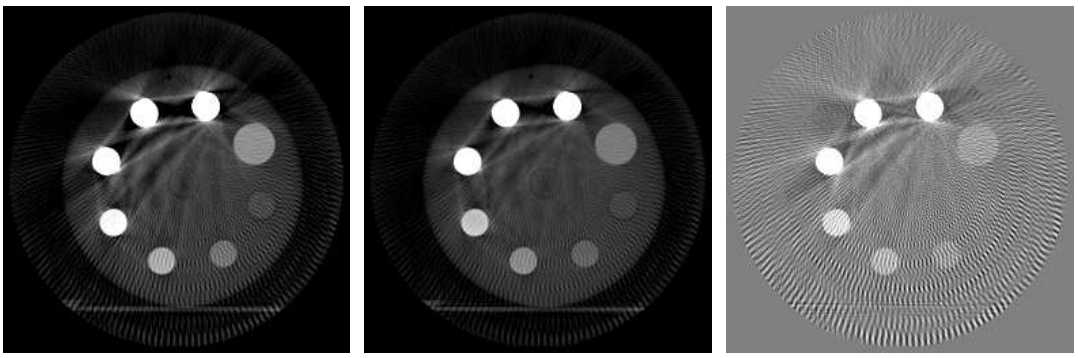

(j) 81 kV; $\sigma_w = 64.85$ HU (k) 125 kV; $\sigma_w = 42.13$ HU (l) Difference (j)-(k)

Figure 7. Axial slice of fast kV-switching scans in first and second column (C 2300 HU, W 6300 HU) and third column the respective difference slice (C 0 HU, W 1250 HU).

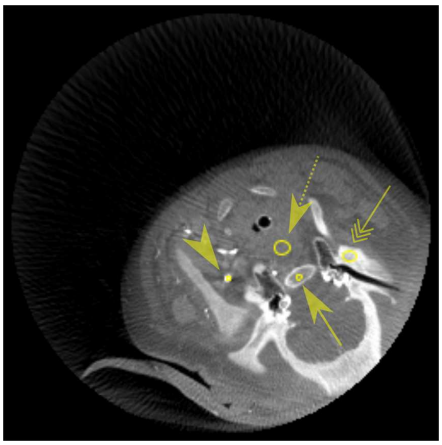

Figure 8. 3D slice of 3D reconstruction of 50% undersampled constant scan of 81 kV with measured ROIs (C 160 HU, W 2000 HU). Arrowhead: contrasted vessel, double arrowhead: dense bone, dashed arrow: soft tissue and normal arrow: bone marrow.

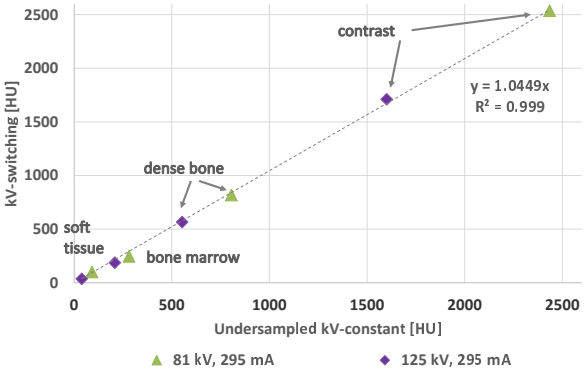

Figure 9. Correlation of HU values measured in the ROIs in the kV-switching and in their respective 50% undersampled constant scans ($R^2 > 0.99$)

than what can be achieved with a conventional CT system where dual-energy acquisitions typically are taken with 80 kV and 140 kV. Therefore, the biggest challenge in the rapid kV-switching with an angiographic C-arm system is the clear separation of the two energy spectra. The separation of the two tube spectra could be improved by a fast rotating copper tin filter that would harden the spectrum for the high-energy data. This requires changes in the angiographic system's hardware and is not yet applicable. Further investigations need to address the performance of the material decompositions task with respect to different dose settings and hence the influence of increase in noise. The current feasibility study was carried out to investigate the system's capability of providing the mechanical basis to perform rapid kV-switching acquisitions.

In order to assure similar exposed 2D X-ray projection images for the low and high-energy data, the detector entrance dose of the low- and high-energy projection images should be as similar as possible. However, the current cannot be changed with up to 30 fps due to the material properties of the filament. This can only be achieved by adapting the pulse width between the adjacent frames. The pulse width limitations right now are a minimal pulse width of 3.2 ms and a maximum pulse width of 12.5 ms.

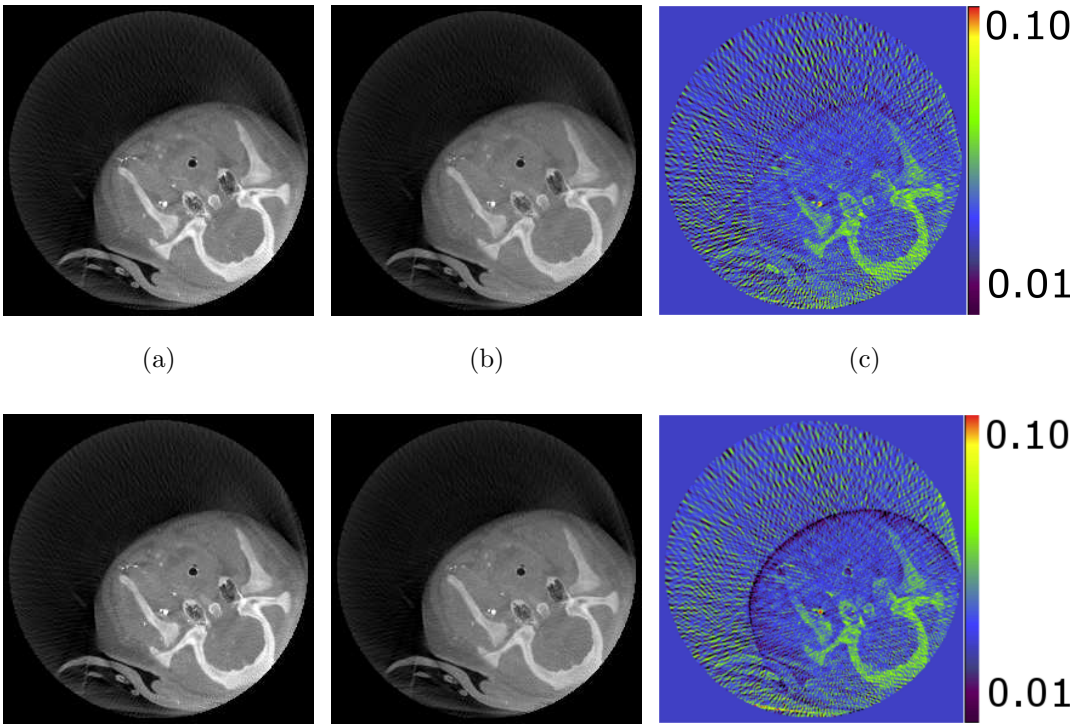

Figure 10. Axial slice of different 3D reconstructions, (a) fast kV-switching 81 kV scan (C 160 HU, W 2000 HU). (b) Fast kV-switching 125 kV scan (C 160 HU, W 2000 HU). (c) Dual-energy index (DEI) image of fast kV-switching 81/125 kV scan. (d) Undersampled kV-constant 81 kV scan (C -460 HU, W 1070 HU). (e) Undersampled kV-constant 125 kV scan (C 160 HU, W 2000 HU) and (f) DEI image of undersampled kV-constant scans.

Overall, further investigations need to address more complex material decomposition specific algorithmic development [22–26], as well as 3D image quality improvements to reduce the undersampling artifacts [27].

V. CONCLUSION

In this paper, the feasibility of fast kV-switching for dual-energy imaging using an angiographic C-arm CT system was investigated. The tube potential was switched between adjacent frames during a 3D rotational scan during detector readout at 30 fps. The evaluation of the tube voltage stability during a fast kV-switching scan was compared to the respective kV-constant scan and showed a relative deviation of about $0.27 \pm 0.18\%$. Overall, the requested pulse width and tube current only differ slightly between kV-constant and fast

kV-switching scans. One potential clinical fast kV-switching application in the angiographic suite is to distinguish iodine from water in order to produce virtual digital subtraction angiography data. Therefore, a fast kV-switching scan between 81 kV and 125 kV was used for an experiment using an electron density phantom. An excellent correlation ($R^2 > 0.99$) between HU values in kV-switching and kV-constant scans was observed for various iodine concentrations in an electron density phantom. The lowest bound of iodine concentration that could be accurately detected was 10%. A first *in vivo* pig experiment also confirmed a high correlation between measured HU values in kV-constant and fast kV-switching scans, and allows for the differentiation of iodine, and soft tissue.

ACKNOWLEDGMENTS

The authors gratefully acknowledge funding support from the NIH Shared Instrument Grant S10 RR026714 supporting the zeego@StanfordLab, and Siemens Healthcare GmbH Advanced Therapies. Special thanks also go to Jeremy Heit, MD, PhD and Yamil Saenz for their help with the in vivo pig experiment.

DISCLAIMER

The concepts and information presented in this paper are based on research and are not commercially available.

Potential conflict of interest

Please note that this study was supported by an institutional research grant funded by Siemens Healthcare, Forchheim, Germany. However, the study design, methodology and results were provided by the first author and were independent of any oversight from the company.

---

[1] L. A. Feldkamp, L. C. Davis, and J. W. Kress, "Practical cone-beam algorithm," Journal of the Optical Society of America A **1**, 612–619 (1984).

[2] A. Tognolini, J. Louie, G. Hwang, L. Hofmann, D. Sze, and N. Kothary, "C-arm Computed Tomography for Hepatic Interventions: A Practical Guide," Journal of Vascular and Interventional Radiology **21**, 1817–1823 (2010).

[3] P. Biaggi, C. Fernandez-Golfín, R. Hahn, and R. Corti, "Hybrid Imaging During Transcatheter Structural Heart Interventions." Current cardiovascular imaging reports **8**, 33 (2015).

[4] N. S. Heran, J. K. Song, K. Namba, W. Smith, Y. Niimi, and A. Berenstein, "The utility of DynaCT in neuroendovascular procedures," American Journal of Neuroradiology **27**, 330–332 (2006).

[5] I. Danad, Z. A. Fayad, M. J. Willemink, and J. K. Min, "New Applications of Cardiac Computed Tomography," JACC: Cardiovascular Imaging **8**, 710–723 (2015).

[6] I. Vlahos, R. Chung, A. Chung, and R. Morgan, "Dual-Energy CT: Vascular Applications," American Journal of Roentgenology **199**, 87–97 (2012).

[7] T. Heye, R. C. Nelson, L. M. Ho, D. Marin, and D. T. Boll, "Dual-energy CT applications in the abdomen." American Journal of Roentgenology **199**, 64–70 (2012).

[8] T. G. Flohr, C. H. McCollough, H. Bruder, M. Petersilka, K. Gruber, C. Süβ, M. Grasruck, K. Stierstorfer, B. Krauss, R. Raupach, A. N. Primak, A. Küttner, S. Achenbach, C. Becker, A. Kopp, and B. M. Ohnesorge, "First performance evaluation of a dual-source CT (DSCT) system," European Radiology **16**, 256–268 (2006).

[9] B. Krauss, K. L Grant, B. T Schmidt, and T. G Flohr, "The Importance of Spectral Separation: An Assessment of Dual-Energy Spectral Separation for Quantitative Ability and Dose Efficiency." Investigative Radiology **50**, 114–118 (2015).

[10] A. Graser, T. R. C. Johnson, H. Chandarana, and M. Macari, "Dual energy CT: Preliminary observations and potential clinical applications in the abdomen," European Radiology **19**, 13–23 (2009).

[11] C. H. McCollough, S. Leng, L. Yu, and J. G. Fletcher, "Dual- and Multi-Energy CT: Principles, Technical Approaches, and Clinical Applications." Radiology **276**, 637–653 (2015).

[12] Z. Yu, S Leng, S.M. Jorgensen, Z. Li, R. Gutjahr, B. Chen, X. Duan, A.F. Halaweish, L. Yu, E.L. Ritman, and C.H. McCollough, "Initial results from a prototype whole-body photon-counting computed tomography system," in *SPIE Medical Imaging* (2015).

[13] M. Manhart, R. Fahrig, J. Hornegger, A. Doerfler, and A. Maier, "Guided Noise Reduction for Spectral CT with Energy-Selective Photon Counting Detectors," in *Proceedings of the Third*

CT Meeting (2014) pp. 91–94.

[14] M. Ahmad, R. Fahrig, M. Spahn, J.-H. Choi, N. Köster, S. Reitz, W. Hinshaw, L. Pung, T. Moore, A. Maier, and K. Müller, "First in-vivo experiments with a large field-of-view flat panel photon-counting detector," in *Proceedings of The Fourth International Conference on Image Formation in X-Ray Computed Tomography*, edited by M. Kachelriess (2016).

[15] K. Müller, M. Ahmad, M. Spahn, J.-H. Choi, S. Reitz, N. Köster, Y. Lu, R. Fahrig, and A. Maier, "Towards material decomposition on large field-of-view flat panel photon-counting detectors – first in-vivo results," in *Proceedings of The Fourth International Conference on Image Formation in X-Ray Computed Tomography*, edited by M. Kachelriess (2016).

[16] M. P M Tijssen, P. A M Hofman, A. A R Stadler, W. Van Zwam, R. De Graaf, R. J. Van Oostenbrugge, E. Klotz, J. E. Wildberger, and A. A. Postma, "The role of dual energy CT in differentiating between brain haemorrhage and contrast medium after mechanical revascularisation in acute ischaemic stroke," European Radiology **24**, 834–840 (2014).

[17] Sebastian Feuerlein, Ewald Roessl, Roland Proksa, Gerhard Martens, Oliver Klass, Martin Jeltsch, Volker Rasche, Hans-Juergen Brambs, Martin H K Hoffmann, and Jens-Peter Schlomka, "Multienergy photon-counting K-edge imaging: potential for improved luminal depiction in vascular imaging." Radiology **249**, 1010–1016 (2008).

[18] S. Datta, J.-H. Choi, C. Niebler, A. Maier, R. Fahrig, and K. Müeller, "Dual-Energy C-Arm CT in the Angiographic Suite," in *2015 IEEE Nuclear Science Symposium and Medical Imaging Conference Record (NSS/MIC)* (2015).

[19] R. Fahrig, R. Dixon, T. Payne, R. L. Morin, A. Ganguly, and N. Strobel, "Dose and image quality for a cone-beam C-arm CT system." Medical Physics **33**, 4541–4550 (2006).

[20] Task Group 12 Diagnostic X-ray Imaging Committee, *Quality Control in Diagnostic Radiology*, AAPM Report No.74 74 (AAPM, 2002).

[21] T. R. C. Johnson, B. Krauss, M. Sedlmair, M. Grasruck, H. Bruder, D. Morhard, C. Fink, S. Weckbach, M. Lenhard, B. Schmidt, T. Flohr, M. F. Reiser, and C. R. Becker, "Material differentiation by dual energy CT: initial experience." European Radiology **17**, 1510–7 (2007).

[22] E. Meyer, R. Raupach, M. Lell, B. Schmidt, and M. Kachelrieß, "Frequency split metal artifact reduction (FSMAR) in computed tomography," Medical Physics **39**, 1904 (2012).

[23] S. Faby, S. Kuchenbecker, S. Sawall, D. Simons, H.-P. Schlemmer, M. Lell, and M. Kachelrieß, "Performance of todays dual energy CT and future multi energy CT in virtual non-contrast

imaging and in iodine quantification: A simulation study," Medical Physics **42**, 4349–4366 (2015).

[24] S. Kuchenbecker, S. Faby, S. Sawall, M. Lell, and M. Kachelrieß, "Dual energy CT: How well can pseudo-monochromatic imaging reduce metal artifacts?" Medical Physics **42**, 1023–1036 (2015).

[25] W Zbijewski, G J Gang, J Xu, a S Wang, J W Stayman, K Taguchi, J a Carrino, and J H Siewerdsen, "Dual-energy cone-beam CT with a flat-panel detector: effect of reconstruction algorithm on material classification." Medical Physics **41**, 021908 (2014).

[26] Justin L. Ducote, Tong Xu, and Sabee Molloi, "Optimization of a flat-panel based real time dual-energy system for cardiac imaging," Medical Physics **33**, 1562 (2006).

[27] T. Niu, X. Dong, M. Petrongolo, and L. Zhu, "Iterative image-domain decomposition for dual-energy CT," Medical Physics **41**, 041901 (2014).